npj | climate and atmospheric science

www.nature.com/npjclimatsci

ARTICLE OPEN

Check for updates

Climate change linked to drought in Southern Madagascar

Angela Rigden[1]✉, Christopher Golden[2], Duo Chan[3] and Peter Huybers[4]

Southern Madagascar experienced a prolonged drought over the last five years, but whether these conditions are a manifestation of global climate change has been unclear. Here, we document trends beginning as early as 1980 towards a later rainy-season onset across three distinct remotely sensed indicators: precipitation, soil moisture, and vegetation greenness. All three indicators closely covary, particularly over the last decade when satellite observational resolution and accuracy is greatest. Furthermore, observed soil moisture trends early in the rainy season agree with the mean from CMIP6 historical and SSP5-8.5 simulations, but are distinct from pre-industrial control simulations, implicating anthropogenic changes in radiative forcing as the source of the trends. Physically, these models simulate a poleward migration of the mid-latitude jet that leads to a delay in the seasonal steering of storm tracks over Southern Madagascar. Soil moisture trends driven by anthropogenic forcing made the recent drought significantly more likely over 2017–2022 ($p < 0.01$), and such droughts are expected to become increasingly likely over this century. These results indicate that, although Madagascar has not substantially contributed to global greenhouse gas emissions, farmers in Southern Madagascar will need to adapt to drier conditions early in the rainy season as a consequence of global climate change.

npj Climate and Atmospheric Science (2024)7:41 ; https://doi.org/10.1038/s41612-024-00583-8

INTRODUCTION

Shortfalls in local food production were caused by a multi-year drought in Southern Madagascar, an event that was called the first climate change driven famine[1]. A subsequent analysis by the World Weather Attribution (WWA) group, however, led to a conclusion that climate change played only a limited role in causing the extremely low rainfall between 2019 and 2021[2]. The WWA group focused on two-year running average precipitation to define baseline conditions, in keeping with the prolonged drought in Madagascar, and relied upon precipitation records from ERA5[3] and CHIRPS[4] to estimate the return period of the observed drought. Although ERA5 and CHIRPS are state-of-the art with respect to meteorological reanalyses and precipitation reconstructions, respectively, these products do not definitively monitor multi-decadal trends on account of a dearth of in-situ meteorological data available for Southern Madagascar and changes in observational platforms and coverage[5]. For example, there are only three precipitation gauges in Southern Madagascar that are input to the CHIRPS dataset, and these three stations are representative of coastal climates and incomplete in their record (Supplementary Fig. 1).

Furthermore, alterations in the hydrological cycle with consequence for agricultural outcomes can occur in the absence of annual-average changes, particularly in Southern Madagascar. Precipitation in Southern Madagascar is strongly seasonal (Fig. 1), peaking around 200 mm month^{-1} in January but with climatological values of less than 10 mm month^{-1} in July and August (Supplementary Fig. 2). Since water is limited for much of the year, farming in Southern Madagascar tracks the seasonal cycle of rain[6]. Cereals and cassava, along with other vegetables, are grown during the rainy season, October through February[7]. Cereals and most vegetables are harvested as the rains subside between March and June, whereas cassava is harvested in the dry season, July through September[7]. Surveys of Malagasy farmers indicate that the cycle of rains and attendant cropping calendars are critical determinants of food production[8], in addition to consistent rain throughout the wet season. A later onset of rains exposes crops to greater water stress, delays maturation, and lengthens the lean season[7].

Observational data indicates decadal trends in Southern Madagascar's seasonal hydrologic cycle. Analyses of precipitation gauges in the Southern Madagascar cities of Toliary and Taolagnaro covering 1950–2018 show a trend toward delayed onset of the rainy season[5]. A similar pattern is found in precipitation records in South Africa[9] that have been shown to co-vary with climate in Southern Madagascar[10]. The shift in seasonality across the interior and northeastern regions of South Africa was linked to Hadley cell expansion and the associated poleward shift of storm tracks[9].

In this study, we characterize the role of climate change on seasonal water availability in Southern Madagascar using climate model simulations and diverse observational metrics of water availability. Our analysis is divided into three sections. First, we characterize the seasonal hydrologic fingerprint expected from anthropogenic climate change using forced and control climate simulations. Second, we assess if the seasonal climate change fingerprint is discernible from well-resolved, remotely sensed observational data. Finally, we consider the recent drought in Southern Madagascar in the context of these observational trends and simulated fingerprints.

RESULTS

Climate change fingerprint of trends from simulations

The question of whether hydrologic trends in Southern Madagascar are related to anthropogenic climate change can be assessed in the context of simulations that include anthropogenic forcing relative to control simulations that do not (Fig. 2). Specifically, we evaluate CMIP6 models that output soil moisture in simulations representing pre-industrial control, historically

[1]Department of Earth System Science, University of California, Irvine, 3200 Croul Hall St, Irvine 92697 CA, USA. [2]Department of Nutrition, Harvard T.H. Chan School of Public Health, 677 Huntington Ave, Boston 02115 MA, USA. [3]School of Ocean and Earth Science, University of Southampton, European Way, Southampton S014 3ZH Hampshire, UK. [4]Department of Earth and Planetary Sciences, Harvard University, 20 Oxford St, Cambridge 02138 MA, USA. ✉email: arigden@uci.edu

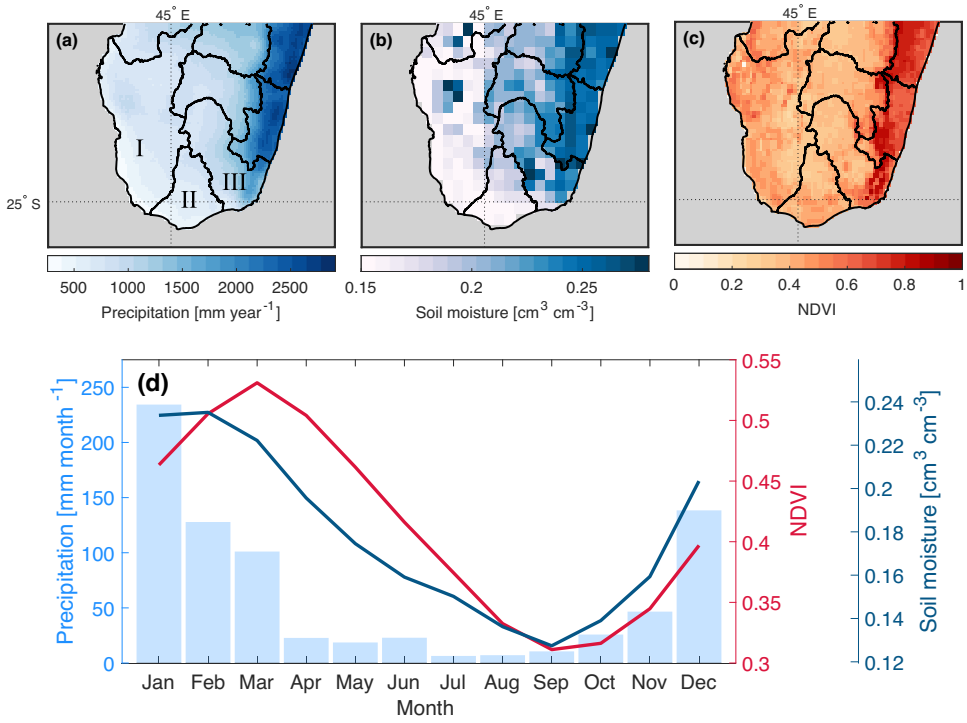

Fig. 1 Observational data. Maps of annual average (**a**) precipitation, (**b**) soil moisture, and (**c**) vegetation greenness as represented by the Normalized Difference Vegetation Index (NDVI), as well as (**d**) the seasonal cycles of precipitation, soil moisture, and NDVI over Southern Madagascar. Values are averaged over 2003–2015. Note that the two right y-axes do not start at zero, and NDVI is from the GIMMS product. We define Southern Madagascar as the three most southern political regions, which are labeled in subplot (**a**): (I) Atsimo-Andrefana, (II) Androy, and (III) Anosy.

forced, and future forced conditions, the latter following the SSP5-8.5 scenario (Supplementary Table 1). Of twelve available models, nine are selected for further analyses based upon their match with historical seasonal variations (see Methods).

Trends in simulated soil moisture between 1982 to 2099 from the forced climate models show a clear seasonal pattern (blue lines in Fig. 2a), with consistent negative trends in soil moisture projected during the onset of the rainy season (Sep-Nov) across all retained models. The average trend across the nine climate models during the onset of the rainy season is a 2.3% decrease in soil moisture per decade (model spread: −4.0% to −1.1%). The sign of the trends across other seasons are model dependent, though the across-model average trend in soil moisture is negative for all months. We refer to the across-model average of monthly trends from the forced climate model simulations as the "seasonal climate change fingerprint" of trends (represented by the navy line in Fig. 2a). Note that a similar seasonal climate change fingerprint emerges from the forced simulations if trends are estimated from 1982 to 2022 (Supplementary Fig. 7), overlapping the observational period, though estimates over this shorter interval are nosier. In contrast, the pre-industrial control simulations show no significant changes in soil moisture for any month (orange shading in Fig. 2a), indicating that the trends in the forced model are a result of anthropogenic climate change.

The underlying dynamics that produce consistent reductions in soil moisture in Southern Madagascar in response to anthropogenic climate change can be understood in the context of a widening of low-latitude overturning atmospheric circulation, or, Hadley cell expansion (see reviews by[11,12]). Hadley cell expansion leads to Southern Madagascar being subject to the drying influence of the descending branch of the Hadley cell for a longer portion of the year. Hadley cell expansion is consistently found in forced CMIP6 models and can be seen in the poleward shift and intensification of maximum descent in the Southern Sub-tropics during July to November (Fig. 3; Supplementary Information). Precipitation declines over these same months in the forced climate simulations (Supplementary Fig. 9), as also found in Southern Africa (e.g.[13]). We also note that the frequency of land-falling tropical cyclones can influence peak summertime rainfall and is expected to decrease as a consequence of global warming[14,15], but this will have greater consequence for Eastern Madagascar than the Southern regions that are our present focus.

Observed trends

We next turn to assessing whether the seasonal climate change fingerprint of trends is observed using records of precipitation, soil moisture, and vegetation greenness (Fig. 1a–c), focusing on the 66% of land area in Southern Madagascar with minimal deforestation (see Methods). These three indicators are tightly coupled in Southern Madagascar due to its semi-arid climate, with precipitation peaking in Austral summer (DJF), near-surface soil moisture following precipitation by about two weeks, and peak greenness occurring in March (Fig. 1d). Although annual average precipitation declines from 1981 to 2022, the onset of the rainy season from September to November is the only season in which the trend in precipitation significantly differs from zero (−2.4 mm month^{-1} decade^{-1}; 90% CI: −4.5 to −0.6 mm month^{-1} decade^{-1}; Fig. 4a–c). This negative trend in water availability during the onset of the rainy period is also apparent in NDVI and soil moisture observations during their respective periods of record (Fig. 4d–f). Furthermore, since the early 2000s, NDVI and soil moisture significantly decline across all four seasons.

In addition to exhibiting similar trends, precipitation, soil moisture, and vegetation greenness exhibit strong interannual correlations. During the interval of common overlap for all our datasets, 2003 to 2015, the correlation between detrended annual precipitation and annual-average NDVI is 0.74 and 0.82, respectively, for the MODIS and GIMMS NDVI products (Fig. 4a). Annual

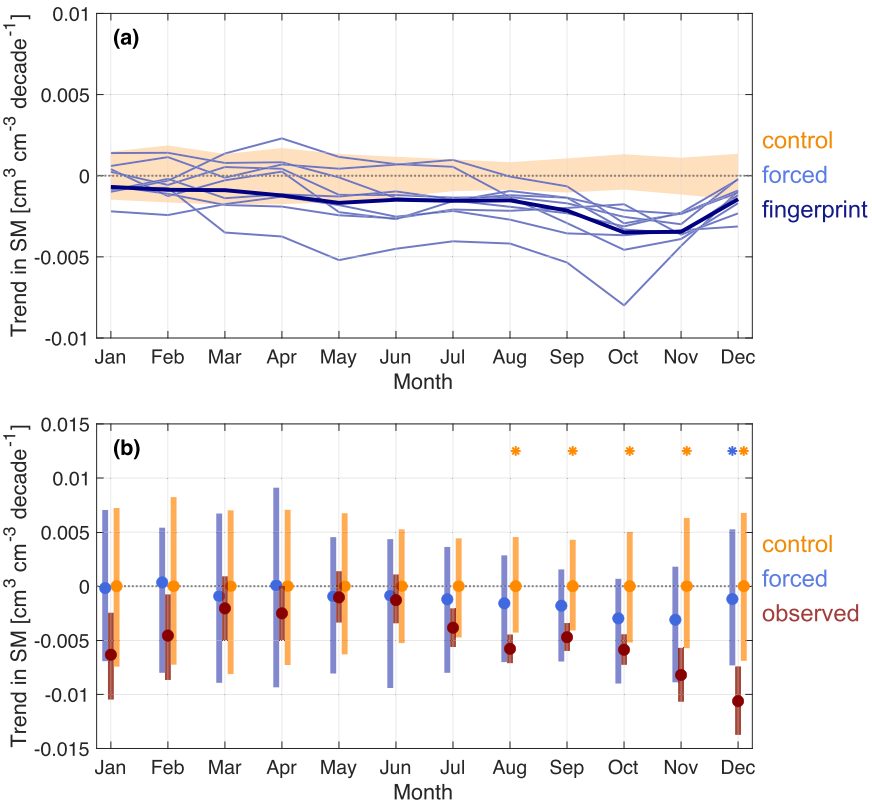

Fig. 2 Climate change fingerprint. a Long-term monthly soil moisture trends estimated from forced simulations ("forced"; blue lines representing individual model runs; navy line representing the across model average, which we refer to as the seasonal climate change fingerprint) and pre-industrial control simulations ("control"; orange shading representing 90% confidence intervals). Trends are estimated from 1982 to 2099 for the forced climate model simulations and over an analogous 118-year time interval for the pre-industrial control simulations. **b** Trends of 41-year length from pre-industrial control simulations (sampled from year 10 to 500; orange), forced model runs (sampled from 1982 to 2099; blue), and proxy soil moisture observations (1982 to 2022; red; see Section 1.2 for a description of proxy soil moisture). Confidence intervals represent the 5th and 95th quantiles of the sampled trends (see Methods), with the median represented by a circle. Note that the confidence intervals for the climate model simulations (forced and control) represent climate variability, while the confidence intervals for the observations represent error in the trend estimation. Asterisks indicate that the sampled trend distribution of the climate model simulations (control or forced) are statistically different from the sampled trend distribution of the observations ($p < 0.05$, one sided test with an alternate hypothesis of a drying trend). We find similar results when trends are estimated at the seasonal scale (Supplementary Fig. 8).

values are computed from September to August in order to center them on the rainy season. Slightly higher correlations are obtained between soil moisture and NDVI, with values of 0.79 and 0.85 for MODIS and GIMMS. Isolating the rainy-season onset months, September through November (Fig. 4b), gives only slightly lower correlation between soil moisture and NDVI of 0.70 and 0.76 for GIMMS and MODIS, but much lower values for precipitation of 0.29 for both NDVI satellite products. Lower correlations involving precipitation may reflect uncertainty in precipitation records, greater variability in seasonal timing, and lags between precipitation and vegetation greenness.

Based on the expectation that soil moisture will determine greenness in Madagascar[16] and the high empirical correlations, we use NDVI to reconstruct soil moisture from 1982 to 2022, and leverage these long-term soil moisture estimates in our attribution analysis. Soil moisture is reconstructed by fitting a lag-linear model of monthly NDVI to soil moisture observations over their common period from 2003 to 2022. A best fit between NDVI and soil moisture is found when NDVI is made to lag by one month (Supplementary Fig. 14). The model is tested using cross validation, and we find good performance across Southern Madagascar (Supplementary Fig. 10). We refer to the trends in estimated soil moisture over the 41-year period as "proxy soil moisture" trends, in contrast to those obtained from more direct observations or simulations.

Attribution of trends and recent drought to anthropogenic forcing

The seasonal pattern of proxy soil moisture trends resembles the fingerprint from forced simulations (Fig. 2b), with declines in proxy soil moisture evident at the end of the dry season and onset of the rainy season. It is useful to quantitatively evaluate how much more likely the proxy soil moisture trends are under anthropogenic forcing relative to pre-industrial variability. Whereas fingerprint techniques have generally opted for projecting onto a scalar quantity for distinguishing between forced and internal variability[17], it is also possible to jointly evaluate the seasonal structure of trends (see Methods and Supplementary Information).

Our approach captures the covariance among seasonal trends through fitting a multivariate normal distribution to seasonal soil moisture trends obtained from forced simulations. A second multivariate normal is fit to seasonal trends from pre-industrial simulations. Evaluating the likelihood ratio of the seasonal proxy soil moisture trends (1982 to 2022) conditional on the forced versus pre-industrial fits indicates that the proxy soil moisture trend structure is 100 times (90% CI: 5-2683 times) more likely as a result of anthropogenic forcing. We thus conclude that the proxy seasonal trends are attributable to anthropogenic climate change.

A complimentary analysis is used to evaluate how much more likely each year of the recent drought is as a consequence of anthropogenic forcing. Analogous to our trend attribution, we fit a

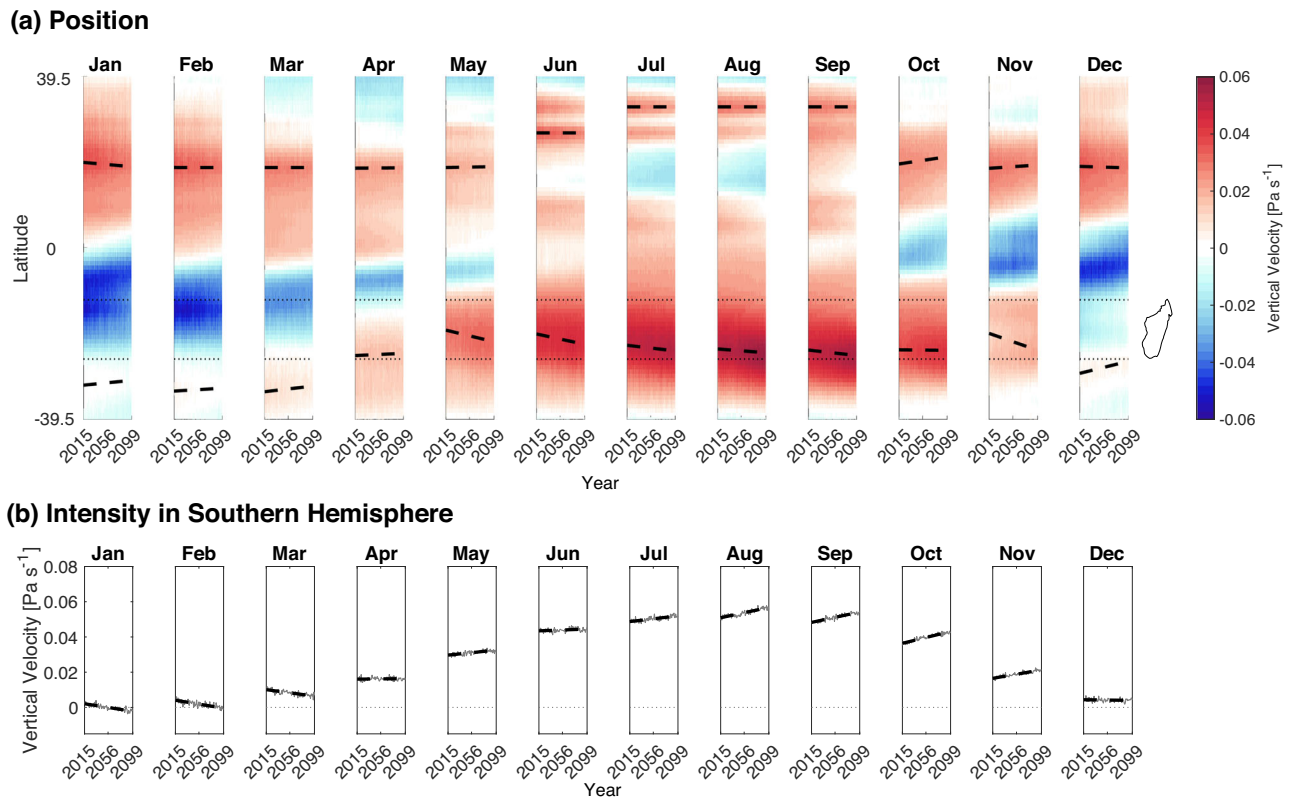

Fig. 3 Projected changes in atmospheric circulation. a Zonally averaged (39.5-59.5°E) monthly vertical velocity at 500 hPa from 46 climate models (267 total ensembles; Supplementary Table 1) from 2015 to 2099 (future projections; SSP5-8.5). The black dashed lines indicate linear trends in the position of the maximum vertical velocity for the Northern Hemisphere (>15°N) and the Southern Hemisphere (<−15°S). The dotted lines show the latitudinal extent of Madagascar, as mapped on the far right axis. **b** Trends in monthly maximum vertical velocity, where the maximum is taken across Southern Hemisphere latitudes. Velocity is measured in units of pressure per second, such that positive values are associated with descending air masses and their attendant clear and dry conditions. See the Supplementary Information for additional details.

multivariate normal to seasonal soil moisture anomalies obtained from a 30-year baseline period, 1970–1999, from forced simulations, as well as a 30-year period centered on the drought years, 2005–2034. Conditional on the CMIP6 simulations, the observed drought conditions between 2017 and 2022 are 15 times more likely as a consequence of anthropogenic forcing (90% CI: 8-27 times). It is also possible to compute the likelihood ratio for individual drought years, in which case 4 out 5 years are individually found to have significantly higher likelihood (Supplementary Table 3). A slight modification of the analysis involves using observed trends prior to the drought, rather than simulated trends, in which case the drought becomes even more likely.

The CMIP6 simulations indicate that the magnitude and seasonality of droughts observed between 2017 and 2022 become increasingly likely further into the future. Likelihood ratios calculated for 30-year intervals ranging between 2000 and 2099 show increasingly high values (Fig. 5), with the 2017-2022 droughts > 1000 times more likely to occur in 2070–2099 than 1970–1999. Higher likelihood of the recent droughts when assessed relative to future simulated conditions under a high-emissions scenario raises the possibility that climate change has proceeded more quickly than simulated by the CMIP6 models with respect to the hydrologic conditions of Southern Madagascar.

DISCUSSION

There are a number of potentially confounding issues associated with the use of remotely-sensed observations, the influence of anthropogenic forcing agents in addition to greenhouse gases, and biases associated with climate model simulations that merit further consideration.

The proxy soil moisture trends we estimate from 1982 to 2022 are based on NDVI and can, obviously, be affected by changes in land use. Deforestation is prevalent in Madagascar and can be correlated with drought conditions because, for example, farmers may attempt to offset yield losses by expanding their farm size through burning[18]. We mitigate the influence of deforestation by masking out regions with moderate to high rates of deforestation[19] based on forest cover maps from 1973 and 2017. Annual deforestation maps are unavailable at high accuracy over the period of record[20]. This approach may not fully account for the influence of small-scale vegetation disturbances or seasonal disturbances, such as seasonal burning that peaks in the late dry season and early wet season[21]. The fact that the trends in rainfall, soil moisture, and NDVI during September to November are consistent, however, points to atmospheric causes and the spatial homogeneity of drying points away from local land-use change, which would be expect to be clustered nearer population centers (Supplementary Fig. 12).

It is also possible that local and non-local deforestation has indirectly affected trends in water availability via interactions with the atmosphere, as deforestation tends to cause warming and drying via reductions in precipitation[22]. Studies from the Amazon reveal that deforestation and the associated decline in transpiration can induce delays in the rainy season onset by altering the chain of atmospheric processes required for rain initiation[23,24]. But transpiration at the end of the dry season in the Amazon is much larger than that in Southern Madagascar, suggesting that the

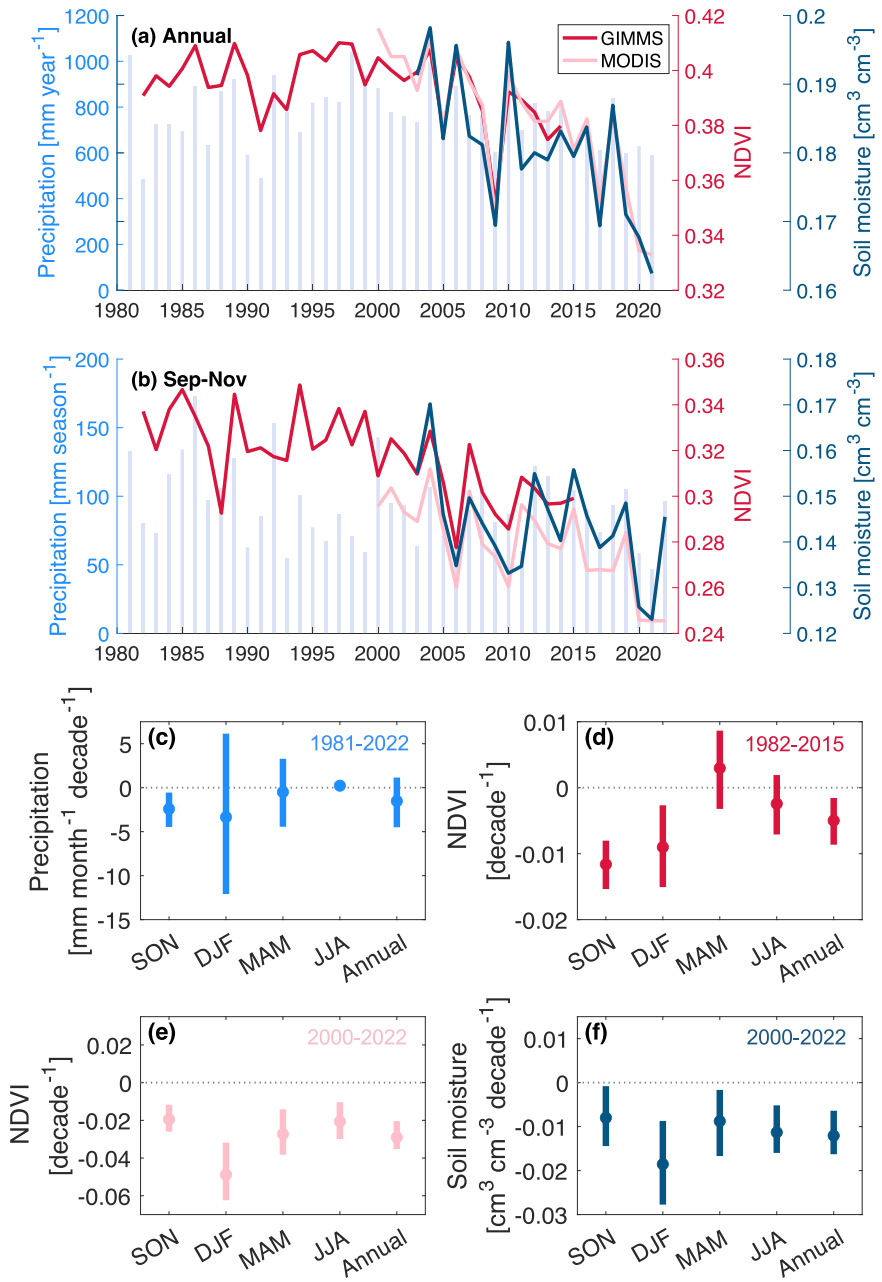

Fig. 4 Trends in observational data. Time series of (**a**) annual average (from September to August) (**b**) and rainy season (from September to November) precipitation, vegetation greenness (NDVI), and soil moisture. **c** Trends for each variable for annual and rainy-season averages. Confidence intervals represent the 5th and 95th quantiles of trends via bootstrapping with 1000 samples, while the dots represent the median (see Methods). Trends are estimated over regions of minimal deforestation.

decrease in transpiration associated with deforestation would have an enhanced role in delaying the onset in the Amazon relative to this region. Model simulations suggest that a complete deforestation of a much larger region in Africa—the Guineo-Congolian region and Eastern Coast of Madagascar—would result in a shortening of the rainy season in Southern Madagascar by approximately 1 to 2 weeks[25]. Deforestation, both local and non-local, may be compounding emission-driven climate change, leading to observed trends that are larger in magnitude than the seasonal climate change fingerprint. Carbon fertilization may also affect trends in vegetation greenness and soil moisture, though the observed concurrent decline in vegetation greenness and soil moisture during the rainy season onset suggests carbon fertilization is not a strong driver of trends.

The depletion of the Antarctic ozone hole may also affect trends in soil moisture[26] through Hadley cell expansion in the Southern Hemisphere that is independent of and in addition to that associated with greenhouse-gas driven warming[27]. Our proxy soil moisture trends, however, are estimated from 1982 to 2022 and span differing trends in ozone hole area, with the first half of the time series (1982 to early 2000s) marked by ozone hole expansion and the second half of the time series (early 2000s to 2022) marked by ozone hole stabilization and recovery[28]. Trends in proxy soil moisture show decreases across both these intervals, indicating that the ozone hole dynamics are not a major driver.

There are a number of model biases that could influence the representation of soil moisture trends and attributions to anthropogenic forcing. Changes in synoptic-scale rainfall systems,

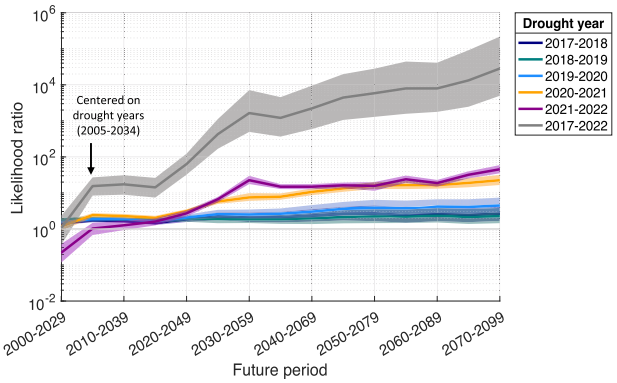

Fig. 5 Drought attribution. Likelihood ratios of recently observed drought conditions in Southern Madagascar for various 30-year intervals covering the present and future relative to a historical baseline from 1970--1999. Ratios are given for individual drought years (colors) and their combination (gray), and shading indicates the 95% confidence interval. Calculations are made using a seasonal climate change fingerprint attribution method based on model simulations only (i.e., not updated using observed trends; See Methods and Supplementary Information for further details).

such as tropical temperate troughs, substantially contribute to intraseasonal rainfall variability in arid regions of southern Africa[29], like Southern Madagascar. The climatology of tropical temperate troughs, including the number, intensity, and positioning, has been shown to vary widely across the CMIP5 models[30], raising questions whether their changes are adequately captured in forced simulations. As another example, the seasonal development of the Mozambique Channel Trough is relevant for channeling moisture transport from the Indian Ocean toward Madagascar[31], but whether CMIP-class models sufficiently represent trough development can be questioned, including on the basis of needing to account for orographic influences that are only coarsely resolved. Nevertheless, a wide variety of model simulations show a consistent delay in the rainy season across Southern Africa in response to anthropogenic forcing. Forced simulations from CMIP5 consistently show a delay in the rainy season across Southern Africa, including Southern Madagascar[32], in agreement with our results based upon CMIP6 simulations. Analyses from downscaled climate model simulations, which better resolve topography, also indicate a decline in Southern Madagascar precipitation during the onset of the rainy season[33,34]. Consistency across models of different generations and resolutions points to Hadley cell expansion as a robust underlying mechanism for causing drying during the onset of Southern Madagascar's rainy season.

In summary, multiple indicators of rainfall and soil moisture indicate long-term trends culminating in recent drought conditions in Southern Madagascar, despite potential biases and uncertainties. Furthermore, observations show patterns of change in water availability that are consistent with climate model simulations, suggesting that anthropogenic climate change is likely altering the seasonal hydroclimatology of Southern Madagascar. Our results suggest that the long-term trends contribute to the recent drought in Madagascar, with the magnitude of the contribution varying depending on details of the calculation. For example, anthropogenic forcing made the drought from September 2019 to August 2020 1.9 times (90% CI: 1.6-2.2 times) more likely, as judged using only simulations, or 4.8 times (90% CI: 2.3-10 times) if simulations are updated using observed trends. It may be that the observed trends are amplified by changes in land use, both directly and indirectly via land-atmosphere interactions, and possibly affected by the formation and recovery of the ozone hole, though none of these appear a dominant driver. The fact that foregoing analyses found little indication of anthropogenic influence on the current drought[2] can be understood in that the climate change fingerprint is muted when averaged annually. Decreases during the early rainy season tend to offset increases during the peak rainy season, shortening the period over which precipitation falls and impacting prospects for agriculture.

Madagascar is estimated to have contributed to global mean surface temperature rise by < 0.01 °C through emissions, whereas the United States, China, and the European Union are estimated to have contributed 0.28 °C, 0.20 °C, and 0.17 °C, respectively[35]. Although Madagascar plays a minimal role in driving global climate change via greenhouse gas emissions, aerosols, and ozone depletion, we find that anthropogenic forcing, as represented in the SSP5-8.5 scenario, is very likely driving shifts in the hydrologic cycle that have major implications for Malagasy agriculture. Adapting to these shifts in the hydrologic cycle may be feasible, for example, through improved water management strategies, innovative farming practices, and public health intervention, but these adaptations will require resources. It remains legally unclear who should provide these resources[36], but efforts to establish climate change accountability are ongoing, for example, by the Climate Vulnerable Forum and the recent COP27 fund for vulnerable countries.

METHODS

Observational data

Monthly average NDVI observations are from two sources: (1) NOAA's Global Inventory Monitoring and Modeling System (GIMMS) version number 3g.v1[37–39] and (2) MODIS/Terra MOD13C2 version 6. The NDVI data from GIMMS data spans from July 1981 to December 2015, while the NDVI data from MODIS spans from February 2000 to present. Monthly NDVI from GIMMS and MODIS are provided globally at 1/12th of a degree and 0.05-degree spatial resolutions, respectively.

Soil moisture data are from the European Space Agency's Climate Change Initiative (ESA CCI) soil moisture product (v08.1)[40,41]. This global product combines single-sensor active and passive microwave observations to estimate 0.25-degree soil moisture from 1979 to 2022. Remotely sensed soil moisture is sensitive to moisture in the near-surface, typically thought to be from 0-5 cm, though recent research has shown that microwave measurements may actually sense deeper into the root-zone, especially for grasslands and croplands[42]. While merging different instruments facilitates a longer period of record, issues of temporal homogenization arise. Most notably, different sensor characteristics have been found to induce temporal shifts that may lead to false trends[43]. Furthermore, the frequency of soil moisture observations at a particular location is inconsistent over the period of record. For example, the number of soil moisture observations significantly increases in July 2002 with the incorporation of passive microwave data from the Advanced Microwave Scanning Radiometer for EOS (AMSR-E) instrument aboard Aqua. To minimize errors associated with large observation gaps, we restrict our analysis to after the incorporation of AMSR-E (2003-2022).

We characterize deforestation, which is the leading driver of land cover change in Madagascar, using maps of forest cover[19]. The forest cover maps combine estimates of annual global tree cover loss[44] with seven historical national forest cover maps for years 1953, 1973, 1990, 2000, 2005, 2010, and 2017. The updated forest cover maps[19] specify the presence or absence of forest at a 30-m spatial resolution across Madagascar for each of the seven years with historical forest cover maps. From 1973 to 2017, the updated forest cover maps show a 34% decrease in forest cover over Southern Madagascar. Across all regions in Madagascar, including the three southern regions in Southern Madagascar, the dominant driver of tree cover loss is shifting agriculture[44]. We

estimate fractional forest cover at analogous 0.25-degree resolution to the ESA CCI soil moisture observations for years 1973 (Supplementary Fig. 11a) and 2017 (Supplementary Fig. 11b). Grid boxes with minimal deforestation are defined as those whose forest fraction decreases by less than 0.15 from 1973 to 2017, which is approximately 66% of the land area in Southern Madagascar (Supplementary Fig. 11c–d).

Climate model simulations

We use historical (1850 to 2015) and future (2015 to 2100) simulations of near-surface (0-10 cm) soil moisture from twelve different climate model runs in the Coupled Model Intercomparison Project Phase 6 (CMIP6; "mrsos" in the CMIP6 archive; see Supplementary Table 1 for list of models and ensembles). Models were selected based on data availability in Google cloud (accessed March 10, 2023). Simulations of soil moisture are from both the high emission scenario (SSP5-8.5) and pre-industrial control runs (piControl). Monthly soil moisture simulations are regridded from their native spatial resolution to a consistent 0.5-degree resolution.

We assess the seasonal cycle and annual spatial pattern of soil moisture from twelve CMIP6 runs with pre-industrial control, historical, and SSP5-8.5 experiments (eleven models, one of which with two ensemble members; Supplementary Table 1). With respect to seasonality, all twelve of the forced simulations (historical and SSP5-8.5) well capture the current (1990–2020) seasonality of soil moisture (Supplementary Fig. 4a). However, three of the twelve models (EC-Earth3-Veg, EC-Earth3, MIROC-ES2L) show unrealistic seasonal cycles in the pre-industrial control simulations, with soil moisture peaking in September or October (Supplementary Fig. 4b), so they are excluded from the remaining analysis. The absolute magnitude of soil moisture varies substantially by model (Supplementary Fig. 4), as expected due to across model variations in precipitation, parameterization schemes, and the underlying land surface models[45]. All of the climate model simulations show lower annual average soil moisture in the southern region of Madagascar relative to the central and northern regions (Supplementary Fig. 5). However, only five of nine model runs exhibit higher annual average soil moisture along the length of the eastern coast, despite this region being well known to receive abundant orographic precipitation. The remaining model runs simulate higher annual average soil moisture in the central region of the country. Indeed, accurate simulation of rainfall is often limited by the resolution of simulations, particularly in areas with complex topography[46], among other factors.

Trends

We estimate trends in observations (NDVI, soil moisture, and precipitation), proxy soil moisture (Eq. (1)), and simulations (soil moisture) using a linear least-squares regression. Trends are estimated annually, monthly, and seasonally, including Sep–Nov (onset of rain), Dec–Feb (peak of rain), Mar–May (end of rain), Jun–Aug (dry spell). Annual averages are centered on the rainy season from Sep-Aug.

Confidence intervals for observations and proxy trends are estimated via bootstrapping, with 90% confidence intervals representing the 0.05 and 0.95 quantiles of 1000 samples (Fig. 4; and red bars in Fig. 2b). These confidence intervals represent the errors associated with the trend estimation, as a distribution of trends is estimated by sampling the values (from 1982 to 2022) with replacement. For climate model simulations, samples of trends are generated by estimating trends every 5-years and the confidence intervals are the 0.05 and 0.95 quantiles of these sampled of trends. For example, in Fig. 2a, the confidence intervals in the pre-industrial control simulations are estimated by estimating 118-year trends every 5 years from year 10 to year 500 for each model run. In Fig. 2b, the confidence intervals represent an analogous procedure, with 41-year trends estimated every 5 years from 1982 to 2099 for the forced simulations and from years 10 to 500 for the control simulations. Trends are taken every 5 years, rather than every year, to avoid temporal correlations, and bootstrapping methods are not used for the climate model simulations to avoid repeating samples. The confidence intervals for the climate model simulations represent the variability in trends– either natural variability (from the pre-industrial control simulations; orange bars in Fig. 2a–b) or forced + natural variability (from the forced simulations; blue bars in Fig. 2b).

Combining NDVI from MODIS and GIMMS

We combine the NDVI from GIMMS (1982 to 2015) and MODIS (2001 to 2022) to estimate a 41-year record. To combine the records, we determine the monthly bias over the period of overlap and adjust the mean in the MODIS data accordingly. Data from GIMMS is used from 1982 to 2015 and MODIS from 2016 to 2022. Note that the observed trend pattern in Fig. 2 is similar when estimated using just GIMMS data from 1982 to 2015. Furthermore, the variability during the overlap period (2001 to 2015) are similar between GIMMS and MODIS (Fig. 4), signifying that the products are capturing similar dynamics in Southern Madagascar.

Inferring soil moisture from NDVI

To estimate soil moisture from NDVI, we first determine the optimal lag (in months) between SM and NDVI by maximizing the correlation of NDVI and SM for each 0.25-degree grid box. Optimal lags are estimated using data from the entire period of overlap between NDVI (GIMMS + MODIS) and soil moisture, or 2003–2022. Lags estimated for individual decades are consistent with one another (Supplementary Fig. 14), and we do not observed systematic trends in this lag, consistent with an assumption of a constant lead-lag relationship. We predict monthly soil moisture at time t from NDVI at time $t-$ lag using non-negative linear least-squares regression,

$$\mathrm{SM}_{t,l} = b + \sum_{i=1}^{N} m_i \mathrm{NDVI}_{t-lag,i} \quad (1)$$

In Eq. (1), SM at grid box l, which is at a 0.25-degree resolution, is estimated using 0.05-degree NDVI observations at sub-grid boxes i whose centers fall within soil moisture grid box edges. Thus, the fit coefficients (m_i) are acting as weights that scale the NDVI observations within each 0.25 degree grid box assuming one constant intercept (b). Predicted soil moisture values inferred from Eq. (1) are similar to those inferred from averaging NDVI over the 0.25-degree grid box, though the latter has less skill given the more limited number of fit coefficients.

To assess the fit of Eq. (1), we fit the model from 2003 to 2022 using the combined NDVI (GIMMS + MODIS) leaving out four sequential years of data, and test the model on those four years, e.g. leave out 2003-2006 in training, and then test the model from 2003 to 2006. We find small increases in mean squared error from the training to testing subsets (Supplementary Fig. 13), with the mean squared error average over undisturbed grid boxes in Southern Madagascar and increasing from 0.0011 cm^3 cm^{-3} in average training subsets to 0.0012 cm^3 cm^{-3} in average testing subsets.

Climate change fingerprint

To evaluate the likelihood of the observed trends in proxy soil moisture relative to those from the control and forced climate model simulations, we apply a climate change fingerprinting method that builds off of longstanding fingerprint methods (e.g.,[17,47]) but also accounts for multiple dimensions, as found in some more recent papers (e.g.,[48]). Specifically, we fit a four-dimensional multivariate normal distribution (MVN) to seasonal features that represents the mean, variance, and covariance for the DJF, MAM, JJA, and SON seasons. We apply the fingerprint to

seasonal trends, rather than monthly trends, to minimize the size of the covariance matrix used to fit the distributions. Accounting for the covariance in trends from one season to the next (Supplementary Fig. 15) is important for purposes of not overstating the significance of the test.

We perform three fingerprint tests involving one approach for trends and two approaches for anomalies. For trends, a MVN is fit to seasonal trends of 41-year length obtained from CMIP6 control simulations, and a second MVN is fit to seasonal trends between 1982 to 2022 from CMIP6 forced simulations. We evaluate the likelihood ratio of the seasonal proxy soil moisture trends by evaluating their likelihood using the forced MVN and dividing by their likelihood obtained using the control MVN. In order to quantify the uncertainty, MVN are repeatedly fit using a bootstrapping approach. For each of 1000 iterations, a linear trend in proxy soil moisture over 1982–2022 is estimated from a sample of the years from 1982–2022 with replacement, and MVN fits are performed for each bootstrapped trend. We report 90% confidence intervals based on the 5th and 95th percentiles of the sample that represent the uncertainties in the fit trends as well as fit MVN. Although we report confidence intervals to give an indication of the full distribution, our hypothesis test is one-sided, with a null that anthropogenic forcing is not associated with a trend or anomaly, and an alternate that there is a trend toward drought or the occurrence of drought. Thus, a trend observed to be more negative than the 5th percentile is significant at $p < 0.05$, whereas a trend above the 95th is insignificant.

Our main approach to estimate the likelihood of the recent droughts relative to a baseline climate involves fitting MVN to seasonal soil moisture anomalies over 30-year intervals from a 1970–1999 baseline period and a 2005–2034 recent period. For each year of the drought, we evaluate the likelihood ratio of the seasonal anomalies in proxy soil moisture during the drought conditional on seasonal anomalies during the baseline period versus the current interval. Multiplying likelihoods across each of the 5 drought years gives an overall likelihood ratio (see Approach 1 in Supplementary Table 3). In order to assess how the likelihood of the observed droughts changes as a function of time, we also compute likelihood ratios using our main approach for 30-year periods between 2000 and 2099, with 5-year increments (e.g. 2000–2029, 2005–2034, ..., 2070–2099; see Fig. 5).

In a second approach, we modify the input data such that the multivariate normal distributions for the baseline (1970–1999) and recent (e.g. 2005–2034) conditions are fit based on the observed trend in proxy soil moisture. Specifically, we use the covariance from the main approach but update the mean using the baseline and drought conditions predicted from a linear regression of proxy soil moisture from 1982 to 2017. The baseline mean is set to the predicted 1982 conditions and the future mean is set to the extrapolation of the trend for each drought year. The multivariate normal distributions are evaluated at the seasonal proxy soil moisture observed for each year of the drought, from which likelihood ratios are computed (Approach 2 in Supplementary Table 3).

We use anomalies in our drought calculations, rather than absolute magnitudes, because soil moisture magnitudes vary across CMIP6 models. Anomalies in the forced simulations are estimated for each model and season by subtracting the seasonal average of the baseline conditions. On account of our proxy soil moisture time series not extending back to 1970, we estimate anomalies for each season by fitting a linear least squares regression over 1982-2017, or the available years prior to recent droughts, and predict and subtract the seasonal conditions in 1982 from the observed drought condition during 2018–2022.

For both drought attribution approaches, MVN are repeatedly fit using a bootstrapping approach, analogous to the trend attribution.

Further information on the trend and drought attribution can be found in the Supplementary Information (Supplementary Figs. 15–17 and Supplementary Tables 2–3).

DATA AVAILABILITY

All data used in this study are publicly available at the following links: soil moisture at https://climate.esa.int/en/projects/soil-moisture/data/, NDVI from MODIS at https://modis.gsfc.nasa.gov/data/dataprod/mod13.php, NDVI from GIMMS at https://iridl.ldeo.columbia.edu, precipitation data at https://www.chc.ucsb.edu/data, deforestation data at https://doi.org/10.18167/DVN1/AUBRRC, and CMIP6 simulations from the Google Cloud.

CODE AVAILABILITY

Code to reproduce our analysis is available from the corresponding author upon reasonable request.

Received: 18 July 2023; Accepted: 24 January 2024;
Published online: 08 February 2024

REFERENCES

1. UN. Madagascar: Severe drought could spur world's first climate change famine (2021). https://news.un.org/en/story/2021/10/1103712.
2. Harrington, L. J. et al. Limited role of climate change in extreme low rainfall associated with southern Madagascar food insecurity, 2019–21. *Environ. Res.: Climate* **1**, 021003 (2022).
3. Hersbach, H. et al. The ERA5 global reanalysis. *Q. J. R. Meteorol. Soc.* **146**, 1999–2049 (2020).
4. Funk, C. et al. The climate hazards infrared precipitation with stations—a new environmental record for monitoring extremes. *Sci. Data* **2**, 150066 (2015).
5. Randriamarolaza, L. Y. A., Aguilar, E., Skrynyk, O., Vicente-Serrano, S. M. & Domínguez-Castro, F. Indices for daily temperature and precipitation in Madagascar, based on quality-controlled and homogenized data, 1950–2018. *Int J Climatol.* **42**, 265–288 (2021).
6. Randriamarolaza, L. Y. A. & Aguilar, E. Rainy season and crop calendars comparison between past (1950–2018) and future (2030–2100) in madagascar. *Meteorol. Appl.* **30**, e2146 (2023).
7. FEWSNET. An early start of the rainy season in the extreme south is favorable for early crop development (2020). https://fews.net/southern-africa/madagascar/food-security-outlook/october-2019.
8. Kruger, L. The timing of agricultural production in hazard-prone areas to prevent losses at peak-risk periods: A case of Malawi, Madagascar and Mozambique. *Jamba: J. Disaster Risk Stud.* **8**, 179 (2016).
9. Roffe, S. J., Fitchett, J. M. & Curtis, C. J. Investigating changes in rainfall seasonality across South Africa: 1987–2016. *Int. J. Climatol.* **41**, E2031–E2050 (2021).
10. Randriamahefasoa, T. S. M. & Reason, C. J. C. Interannual variability of rainfall characteristics over southwestern Madagascar. *Theor. Appl. Climatol.* **128**, 421–437 (2017).
11. Xian, T. et al. Is Hadley Cell expanding? *Atmosphere* **12**, 1699 (2021).
12. Staten, P. W. et al. Tropical widening: From global variations to regional impacts. *Bull. Am. Meteorol. Soc.* **101**, E897–E904 (2020).
13. Burls, N. J. et al. The Cape Town "Day Zero" drought and Hadley cell expansion. *npj Clim. Atmos. Sci.* **2**, 27 (2019).
14. Muthige, M. S. et al. Projected changes in tropical cyclones over the South West Indian Ocean under different extents of global warming. *Environ. Res. Lett.* **13**, 065019 (2018).
15. Malherbe, J., Engelbrecht, F. A. & Landman, W. A. Projected changes in tropical cyclone climatology and landfall in the Southwest Indian Ocean region under enhanced anthropogenic forcing. *Clim. Dyn.* **40**, 2867–2886 (2013).
16. Brown, K. A., Yesuf, G. & Carvalho, F. *The New Natural History of Madagascar* 113–120 (Princeton University Press, 2022).
17. Hegerl, G. C. et al. Detecting greenhouse-gas-induced climate change with an optimal fingerprint method. *J. Clim.* **9**, 2281–2306 (1996).
18. Desbureaux, S. & Damania, R. Rain, forests and farmers: Evidence of drought induced deforestation in Madagascar and its consequences for biodiversity conservation. *Biol. Conserv.* **221**, 357–364 (2018).
19. Vieilledent, G. et al. Combining global tree cover loss data with historical national forest cover maps to look at six decades of deforestation and forest fragmentation in Madagascar. *Biol. Conserv.* **222**, 189–197 (2018).
20. Rigden, A. J., Golden, C. & Huybers, P. Retrospective predictions of rice and other crop production in Madagascar using soil moisture and an NDVI-based calendar from 2010–2017. *Remote Sens.* **14**, 1223 (2022).
21. Frappier-Brinton, T. & Lehman, S. M. The burning island: Spatiotemporal patterns of fire occurrence in Madagascar. *PLoS ONE* **17**, 1–17 (2022).
22. Lawrence, D. & Vandecar, K. Effects of tropical deforestation on climate and agriculture. *Nat. Clim. Change* **5**, 27–36 (2015).

23. Wright, J. S. et al. Rainforest-initiated wet season onset over the southern Amazon. *Proc. Natl. Acad. Sci.* **114**, 8481–8486 (2017).
24. Butt, N., de Oliveira, P. A. & Costa, M. H. Evidence that deforestation affects the onset of the rainy season in Rondonia, Brazil. *J. Geophys. Res. Atmos.* **116**, D11120 (2011).
25. Duku, C. & Hein, L. The impact of deforestation on rainfall in Africa: a data-driven assessment. *Environ. Res. Lett.* **16**, 064044 (2021).
26. Thompson, D. W. J. & Solomon, S. Interpretation of recent Southern Hemisphere climate change. *Science* **296**, 895–899 (2002).
27. Kang, S. M., Polvani, L. M., Fyfe, J. C. & Sigmond, M. Impact of polar ozone depletion on subtropical precipitation. *Science* **332**, 951–954 (2011).
28. Dhomse, S. S. et al. Estimates of ozone return dates from chemistry-climate model initiative simulations. *Atmos. Chem. Phys.* **18**, 8409–8438 (2018).
29. Hart, N. C. G., Reason, C. J. C. & Fauchereau, N. Cloud bands over southern Africa: seasonality, contribution to rainfall variability and modulation by the MJO. *Clim. Dyn.* **41**, 1199–1212 (2013).
30. James, R., Hart, N. C. G., Munday, C., Reason, C. J. C. & Washington, R. Coupled climate model simulation of tropical–extratropical cloud bands over southern Africa. *J. Clim.* **33**, 8579–8602 (2020).
31. Barimalala, R., Desbiolles, F., Blamey, R. C. & Reason, C. Madagascar influence on the South Indian Ocean Convergence Zone, the Mozambique Channel Trough and southern African rainfall. *Geophys. Res. Lett.* **45**, 11,380–11,389 (2018).
32. Dunning, C. M., Black, E. & Allan, R. P. Later wet seasons with more intense rainfall over Africa under future climate change. *J. Clim.* **31**, 9719–9738 (2018).
33. Tadross, M., Randriamarolaza, L., Rabefitia, Z. & Yip, Z. K. Climate change in Madagascar: recent, past and future. Tech. Rep. (Climate Systems Analysis Group, National Meteorological Office, 2008).
34. Barimalala, R., Raholijao, N., Pokam, W. & Reason, C. J. C. Potential impacts of 1.5 °C, 2 °C global warming levels on temperature and rainfall over Madagascar. *Environ. Res. Lett.* **16**, 044019 (2021).
35. Jones, M. W. et al. National contributions to climate change due to historical emissions of carbon dioxide, methane, and nitrous oxide since 1850. *Sci. Data* **10**, 155 (2023).
36. Otto, F. E. L. et al. Causality and the fate of climate litigation: The role of the social superstructure narrative. *Glob. Policy* **13**, 736–750 (2022).
37. Tucker, C. J. et al. An extended AVHRR 8-km NDVI dataset compatible with MODIS and SPOT vegetation NDVI data. *Int. J. Remote Sens.* **26**, 4485–4498 (2005).
38. Tucker, C. J., Pinzon, J. E. & Brown, M. E. Global inventory modeling and mapping studies (ndvi 3g.v1) (2004).
39. Pinzon, J. E. & Tucker, C. J. A non-stationary 1981–2012 AVHRR NDVI3g time series. *Remote Sens.* **6**, 6929–6960 (2014).
40. Dorigo, W. et al. ESA CCI soil moisture for improved earth system understanding: State-of-the art and future directions. *Remote Sens. Environ.* **203**, 185–215 (2017).
41. Gruber, A., Scanlon, T., van der Schalie, R., Wagner, W. & Dorigo, W. Evolution of the ESA CCI soil moisture climate data records and their underlying merging methodology. *Earth Syst. Sci. Data* **11**, 717–739 (2019).
42. Feldman, A. F. et al. Remotely sensed soil moisture can capture dynamics relevant to plant water uptake. *Water Resour. Res.* **59**, e2022WR033814 (2023).
43. Preimesberger, W., Scanlon, T., Su, C.-H., Gruber, A. & Dorigo, W. Homogenization of structural breaks in the global ESA CCI soil moisture multisatellite climate data record. *IEEE Trans. Geosci. Remote Sens.* **59**, 2845–2862 (2021).
44. Hansen, M. C. et al. High-resolution global maps of 21st-century forest cover change. *Science* **342**, 850–853 (2013).
45. Wang, A., Kong, X., Chen, Y. & Ma, X. Evaluation of soil moisture in CMIP6 multimodel simulations over conterminous China. *J. Geophys. Res. Atmos.* **127**, e2022JD037072 (2022).
46. Di Luca, A., de Elía, R. & Laprise, R. Potential for added value in precipitation simulated by high-resolution nested regional climate models and observations. *Clim. Dyn.* **38**, 1229–1247 (2012).
47. Stott, P. A. et al. Detection and attribution of climate change: a regional perspective. *Wiley Interdiscip. Rev. Clim. Change* **1**, 192–211 (2010).
48. Chiang, F., Greve, P., Mazdiyasni, O., Wada, Y. & AghaKouchak, A. A multivariate conditional probability ratio framework for the detection and attribution of compound climate extremes. *Geophys. Res. Lett.* **48**, e2021GL094361 (2021).

ACKNOWLEDGEMENTS

P.H. acknowledges support from the Sahara Project. C.G. acknowledges financial support from Catholic Relief Services.

AUTHOR CONTRIBUTIONS

All authors designed the study and interpreted results. A.R. and D.C. analyzed the data. A.R. and D.C. contributed materials and analysis tools. A.R. and P.H. wrote the paper with input from all authors.

COMPETING INTERESTS

The authors declare no competing interests.

ADDITIONAL INFORMATION

Supplementary information The online version contains supplementary material available at https://doi.org/10.1038/s41612-024-00583-8.

Correspondence and requests for materials should be addressed to Angela Rigden.

Reprints and permission information is available at http://www.nature.com/reprints

Publisher's note Springer Nature remains neutral with regard to jurisdictional claims in published maps and institutional affiliations.